Estimation of Emission During the ATV Re-entry

Iain D. Boyd
University of Michigan

Emission generated by the bow shock formed around the ATV as it re-enters the Earth's atmosphere is estimated using a two-step procedure. First, the flow field formed in front of the cylindrical face of the vehicle, that has a radius of 2.25 m, is computed using one of two techniques: (1) the continuum Navier-Stokes equations are solved using computational fluid dynamics (CFD) [1] at lower altitudes of 50 and 75 km; and (2) the particle-based direct simulation Monte Carlo (DSMC) method [2] is used at the higher altitudes (100 and 125 km). All flow field computations include thermal and chemical nonequilibrium. The freestream flow conditions employed are shown in Table 1. The speeds at given altitudes were calculated by H. Klinkrad (ESA/ESOC) in early June of 2008, from the SCARAB fragmentation model as applied to ATV. The vehicle wall temperatures are calculated iteratively in the DSMC simulations using the assumption of radiative equilibrium, and a maximum wall temperature of 900 K (equal to the melting point of aluminum) is employed in both CFD computations.

Table 1: Freestream flow conditions for ATV re-entry.

h (km)	U (km/s)	T (K)	n [N_2] (m^{-3})	n [O_2] (m^{-3})	n [O] (m^{-3})	n [N] (m^{-3})	n [E-] (m^{-3})
125	7.58	484	1.77e17	2.35e16	5.68e16	1.03e12	1.00e11
100	7.60	191	8.45e18	2.02e18	4.00e17	2.02e11	-
75	7.40	224	4.66e20	1.25e20	-	-	-
50	6.00	271	1.35e22	3.63e21	-	-	-

The flow field solutions along the stagnation streamline (starting at the vehicle surface and moving outwards to the freestream) for species number densities and temperatures are input into the nonequilibrium radiation code NEQAIR [3] to compute the associated radiation. Computation of air plasma radiation uses the Quasi-Steady State (QSS) assumption provided by NEQAIR.

For the two higher altitude cases, emission from potassium and zinc is estimated using the Boltzmann (equilibrium) assumption in NEQAIR due to a lack of detailed excitation rate coefficients. These metals are assumed to arise from the evaporation of the white paint applied to the exterior of the ATV vehicle. Strong emission signals from K-I and Zn-I were measured in the Multi-instrument Aircraft Campaign (MAC) associated with the Stardust Sample Return Capsule entry [4]. The DSMC computations include a flux of potassium and zinc from the surface due to paint evaporation. The surface fluxes of these metals are determined based on the approach developed in the prior Stardust analyses [5] and are expressed as fixed fractions of the total freestream mass flux at each altitude. The estimated emissions from these metals are likely to be over-predicted in the

present analyses due to: (1) the use of the Boltzmann model in NEQAIR that is known to over-estimate emissions in nonequilibrium flow environments; and (2) the use of the same relative mass fractions of evaporation products as were employed in Stardust since the latter entry was at much higher energy likely resulting in higher evaporation rates. In all cases, the emissions are computed over the wavelength range of 350 to 1700 nm and the instrument is assumed to view the front face of the ATV vehicle from a distance of 100 km. Atmospheric extinction is not included in the analysis. The wavelength resolution employed in all NEQAIR calculations is 0.05 nm and a FWHM of 0.5 nm is assumed.

Analysis at 125 km (DSMC)

The flow is very rarefied at this condition with a Knudsen number of 3.5. CFD cannot be applied under these conditions. The DSMC computation employed a mesh of 159x89 cells and about 1 million particles. Figure 1a shows contours of temperature illustrating the very thick, diffuse shock wave formed under this condition. The self-consistent wall temperature computed for this condition is about 450 K. Figures 1b show profiles along the stagnation streamline of temperatures and selected species number densities. These are some of the inputs provided to NEQAIR to compute the emission spectra. The temperature profiles show a very strong degree of nonequilibrium among the energy modes (Tt=translation; Tr=rotation; Tv=vibration; Te=electron). The electron temperature has a strongly nonequilibrium profile due to the assumption that all electrons recombine with ions on the vehicle surface. The number density profiles show that there is almost no air chemistry occurring at this near-collisionless flow condition. There is a small population of electrons in the atmosphere at 125 km altitude [6], and this is the source of electrons that ultimately lead to radiation computed by NEQAIR. Figure 2a shows the computed spectra for: (1) a blackbody at 450 K (the computed wall temperature for this condition); (2) for the air plasma; and (3) for potassium and zinc. Figure 2b shows the same results plotted as astronomical magnitude. There is relatively weak emission from the air plasma at this altitude with a maximum flux density of about 10^{-12} W/m^2/nm. Much stronger signals, on the order of 10^{--8} W/m^2/nm, are predicted to arise from the metallic paint evaporation products.

Analysis at 100 km (DSMC)

The flow is much less rarefied at this condition with a Knudsen number of about 0.05. Figure 3a shows contours of temperature illustrating how, in comparison to the 125 km case, the shock moves closer to the body, becomes less diffuse, and leads to higher peak temperatures. The self-consistent wall temperature computed for this condition is about 750 K. Figures 3b show profiles along the stagnation streamline of temperatures and selected species number densities. The temperature profiles continue to show a strong degree of nonequilibrium, although the electrons now behave more consistently with the other energy modes due to the much higher collision rates experienced at this condition. The

number density profiles indicate finite levels of oxygen and nitrogen dissociation and the formation of electrons in the flow through ionization. There are essentially no electrons in the free stream at this altitude. Figure 4a shows the computed spectra for: (1) a blackbody at 750 K (the computed wall temperature for this condition); (2) for the air plasma; and (3) for potassium and zinc. Figure 4b shows the same results plotted as astronomical magnitude. Once again, the strongest signals are predicted to arise from the metal lines but now there are also stronger signals at low wavelength from N_2+ and a number of atomic O and N lines. There appears to be a good prospect at long wavelengths to determine the surface temperature based on these results.

Analysis at 75 km (CFD)

At this condition, the Knudsen number is about 0.001 and the flow can be computed accurately using CFD. Figure 5a shows contours of temperature illustrating how the shock moves even closer to the body, although the peak temperature is reduced due to a higher level of chemistry. Figures 5b show profiles along the stagnation streamline of temperatures and selected species number densities. The temperature profiles show that the flow is close to thermal equilibrium. The number density profiles indicate finite levels of oxygen and nitrogen dissociation and the formation of electrons in the flow through ionization. Figure 6a shows the computed spectra for: (1) a blackbody at 900 K (the assumed wall temperature representing the melting point of aluminum); and (2) for the air plasma. It is not possible to simulate fluxes of the metals from the surface using the CFD code and in any case most of the paint should have been removed by this stage of the re-entry. Figure 6b shows the same results plotted as astronomical magnitude. The computed spectra show strong features of N_2+ at low wavelength, and a sequence of strong atomic oxygen and nitrogen lines between 700 and 1300 nm.

Analysis at 50 km (CFD)

At this condition, the Knudsen number is about $3x10^{-5}$ and is well into the continuum flow regime where CFD is valid. Figure 7a shows contours of temperature illustrating a reduction in the peak temperature due to the lower free stream velocity at this altitude. Figures 7b show profiles along the stagnation streamline of temperatures and selected species number densities. The temperature profiles show that the post-shock flow is in thermal and chemical equilibrium. The number density profiles again indicate finite levels of oxygen and nitrogen dissociation and the formation of electrons in the flow through ionization. Figure 8a shows the computed spectra for: (1) a blackbody at 900 K (the assumed wall temperature representing the melting point of aluminum); and (2) for the air plasma. Figure 8b shows the same results plotted as astronomical magnitude. The computed spectra show strong features of N_2+ and N_2 at low wavelength and reduced emissions from the atomic lines that result from the lower post-shock temperatures as well as the lower levels of dissociation.

Closing Remarks

The levels of emission predicted in the analyses appear to lie in the range where the Echelle instrument, used previously in the Stardust MAC [4], should be able to resolve many of the features. For example, at 71 km altitude in the Stardust entry, Echelle was able to clearly distinguish many spectral features at measured flux density levels between 10^{-10} and 10^{-7} W/m^2/nm. Early in the ATV re-entry, it appears that strong signals should be detected from paint products. Later in the re-entry, strong emissions from air plasma lines are expected. At low wavelength, strong emissions from molecular bands are predicted. At high wavelength, it should be possible to determine the vehicle surface temperature based on the measured continuum.

The levels of emission (per steradian) generated by the bow shock around ATV will be much lower than those for Stardust due to the significantly lower entry velocity. However, in terms of instrument detection, the flux density for ATV is of similar magnitude to Stardust due to two factors: (1) the ATV is significantly larger than Stardust (factor of 25 larger cross sectional area); and (2) the ATV-MAC is significantly closer to the vehicle (factor of 3-4 times closer). Both of these effects result in a significantly larger solid viewing angle for ATV in comparison to Stardust that counteracts the decreased emission levels.

Acknowledgment

This work was supported by the European Space Agency through a grant from the SETI Institute, as part of the ATV-1 "Jules Verne" Multi-Instrument Aircraft Campaign.

References

[1] Scalabrin, L.C. and Boyd, I.D., "Numerical Simulations of the FIRE-II Convective and Radiative Heating Rates," AIAA Paper 2007-4044, June 2007.
[2] Bird, G.A., *Molecular Gas Dynamics and the Direct Simulation of Gas Flows*, Oxford University Press, 1994.
[3] Whiting, E.E., Park, C., Liu, Y., Arnold, J.O., and Paterson, J.A., “NEQAIR96, Nonequilibrium and Equilibrium Radiative Transport and Spectra Program: User's Manual,” *NASA Reference Publication 1389*, December 1996.
[4] Jenniskens, P., “Observations of the STARDUST Sample Return Capsule Entry with a Slit-Less Echelle Spectrograph,” AIAA Paper 2008-1210, January 2008.
[5] Boyd, I.D., Zhong, J., Levin, D.A., and Jenniskens, P., “Flow and Radiation Analyses for Stardust Entry at High Altitude,” AIAA Paper 2008-1218, January 2008.
[6] Kelley, M.C., *The Earth’s Ionosphere*, Academic Press, 1989.

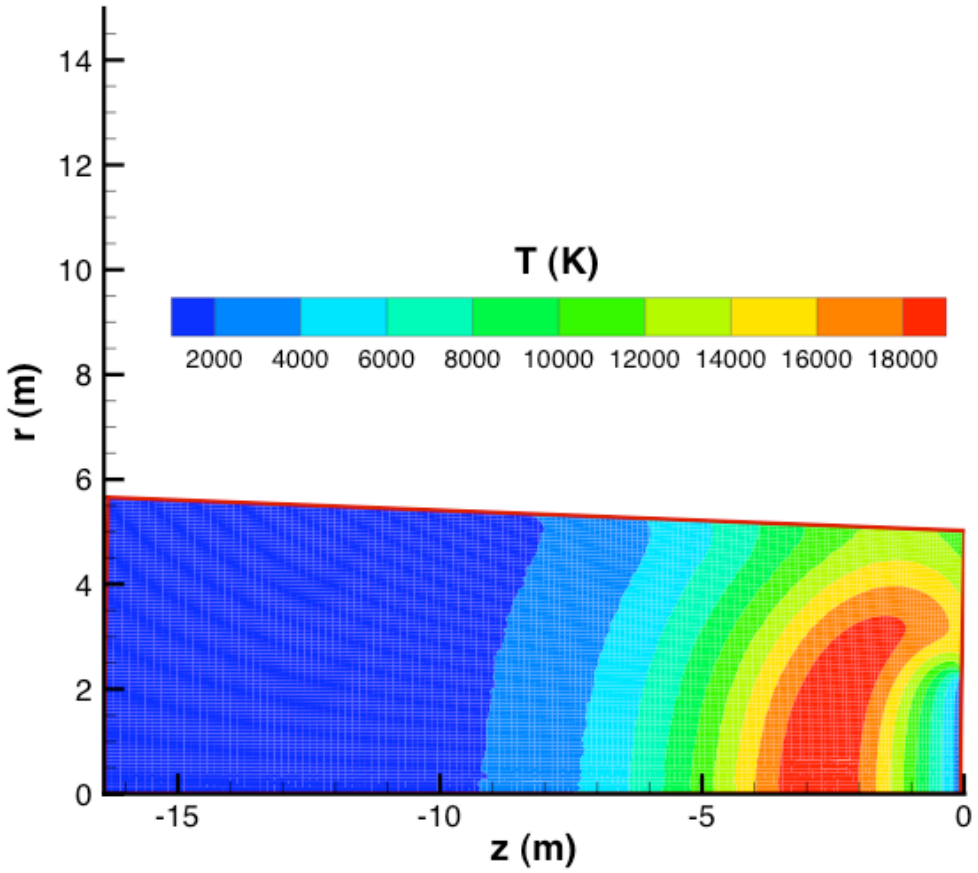

Fig. 1a: Contours of temperature at 125 km (DSMC).

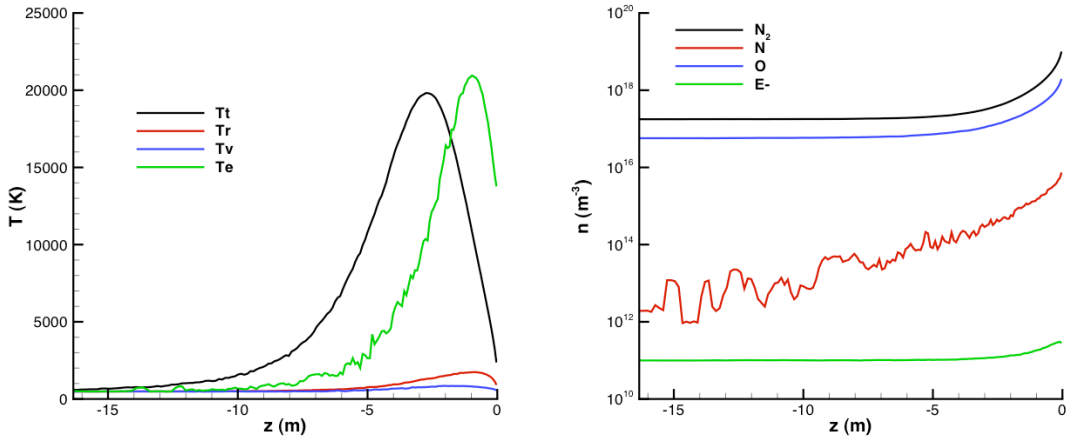

Fig. 1b: Profiles along the stagnation streamline at 125 km of: (a) temperatures; (b) selected species number densities.

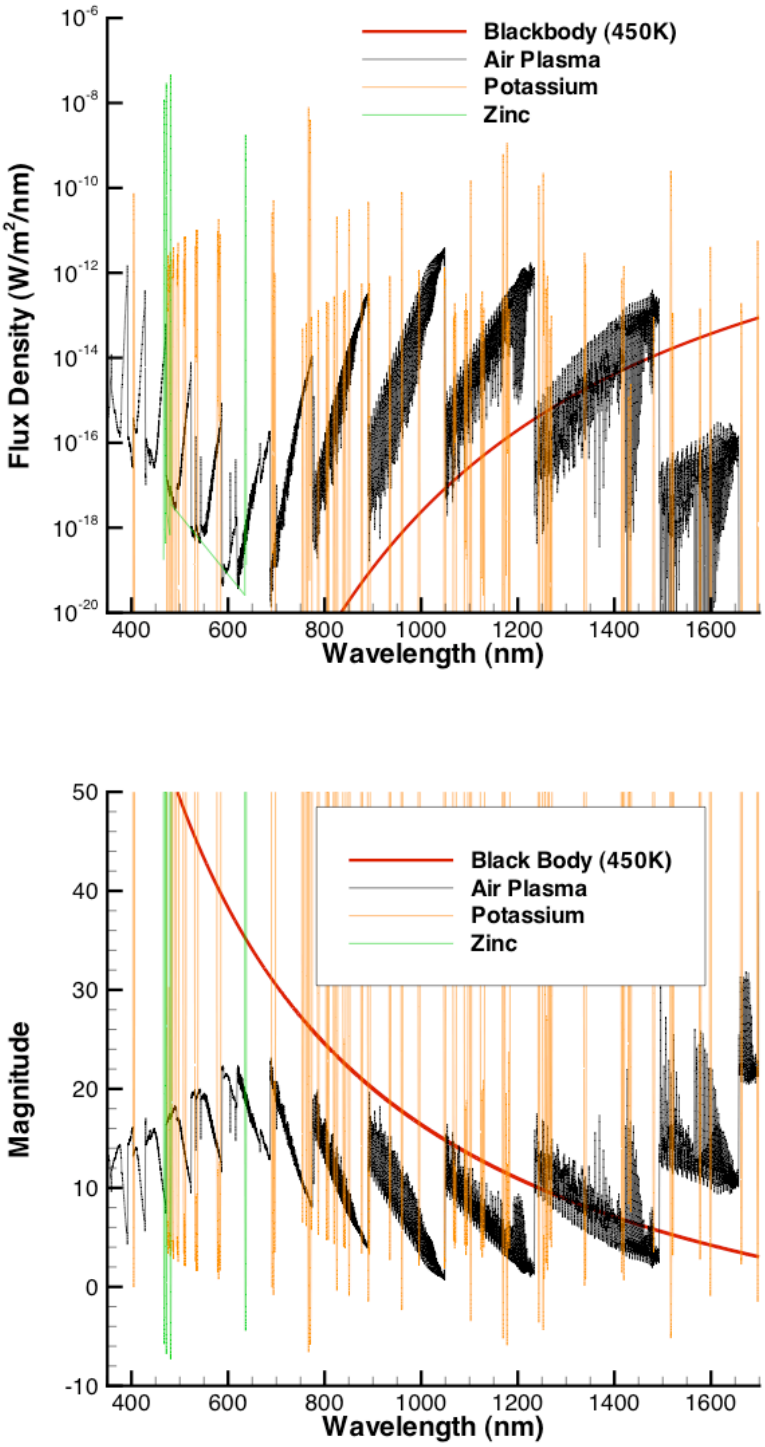

Fig. 2: Estimated radiation at 125 km: (a) flux density; (b) magnitude.

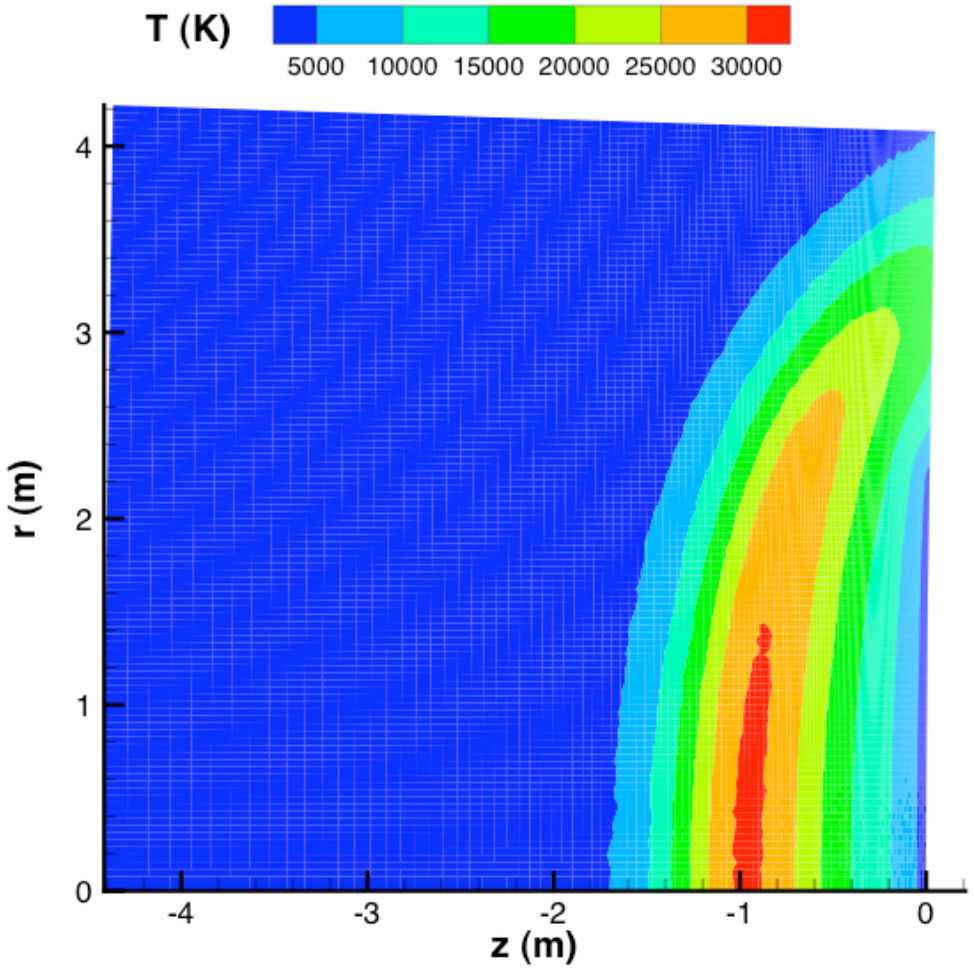

Fig. 3a: Contours of temperature at 100 km (DSMC).

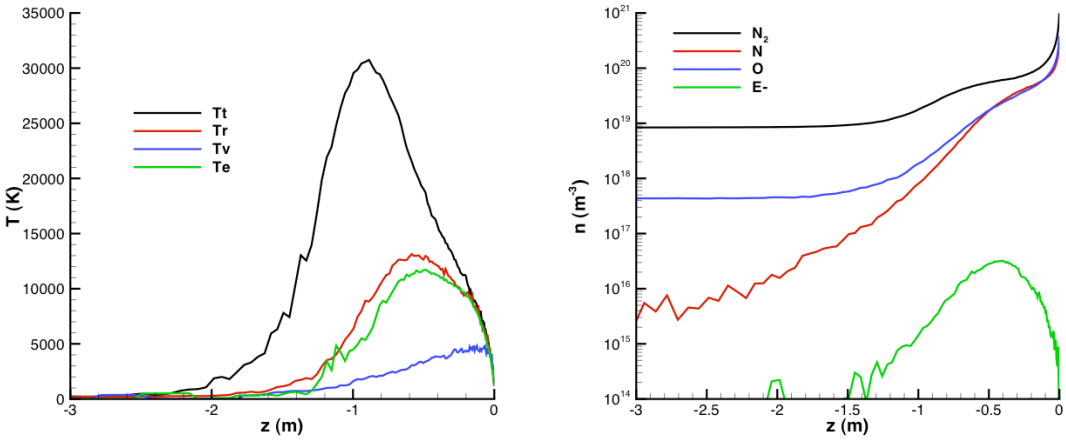

Fig. 3b: Profiles along the stagnation streamline at 100 km of: (a) temperatures; (b) selected species number densities.

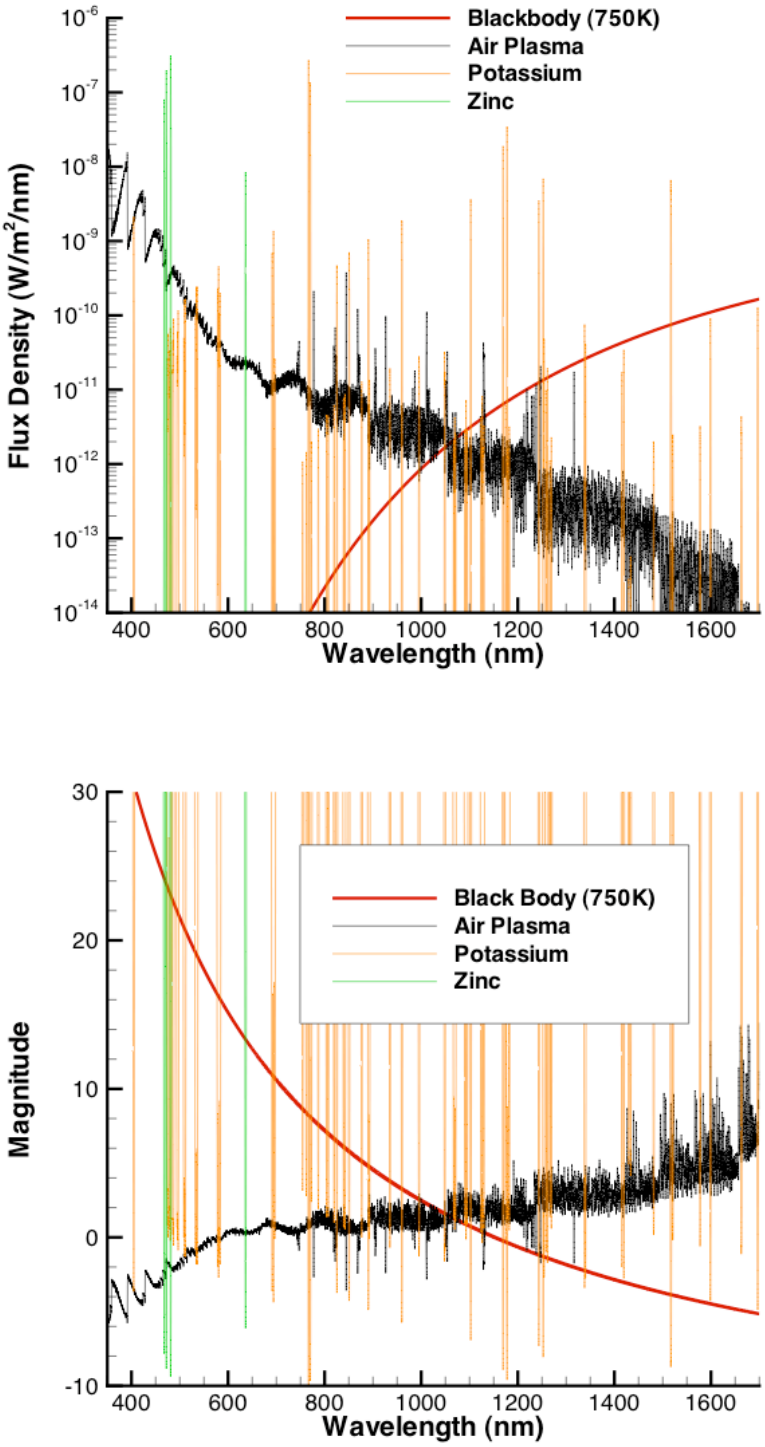

Fig. 4: Estimated radiation at 100 km: (a) flux density; (b) magnitude.

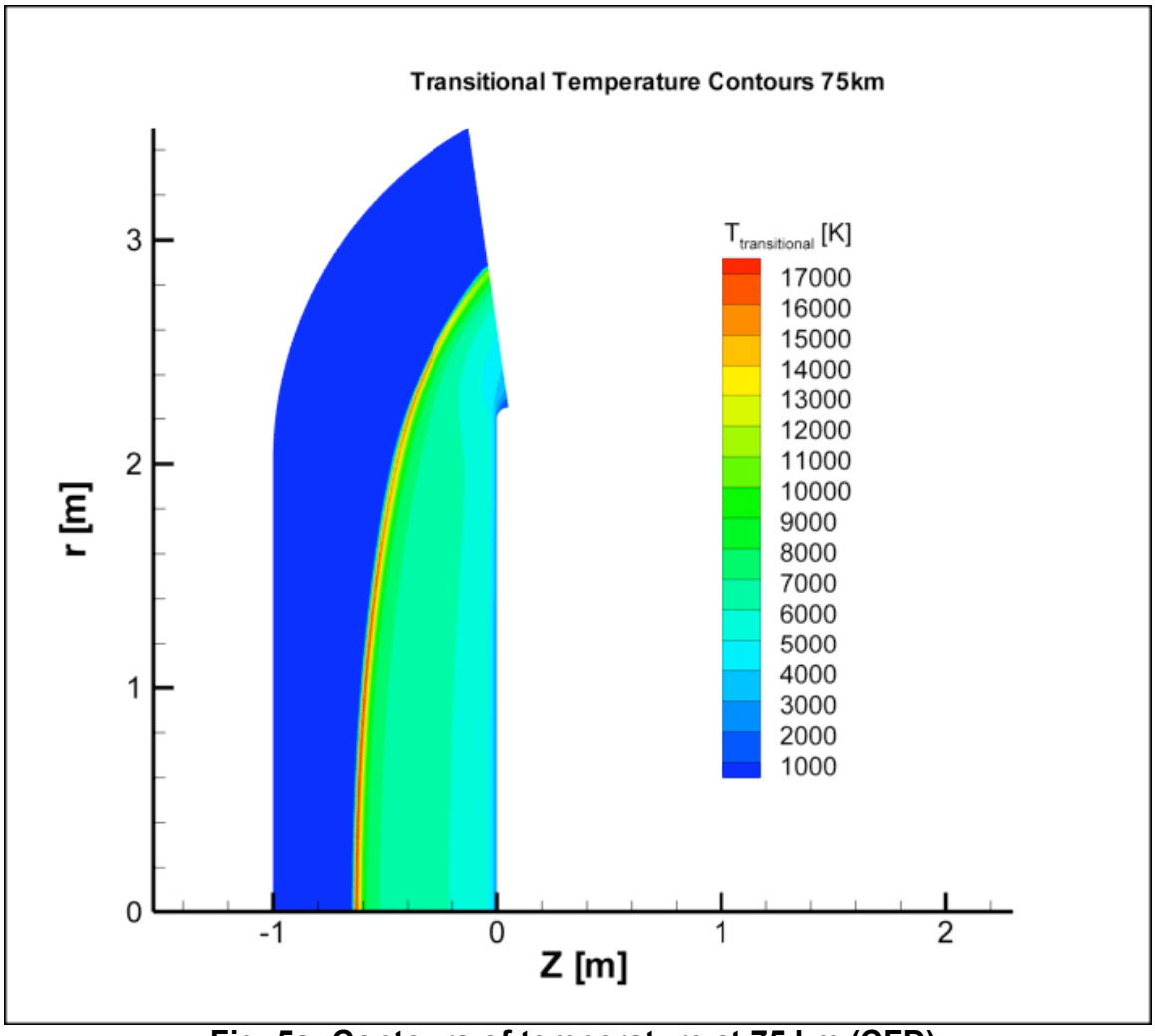

Fig. 5a: Contours of temperature at 75 km (CFD).

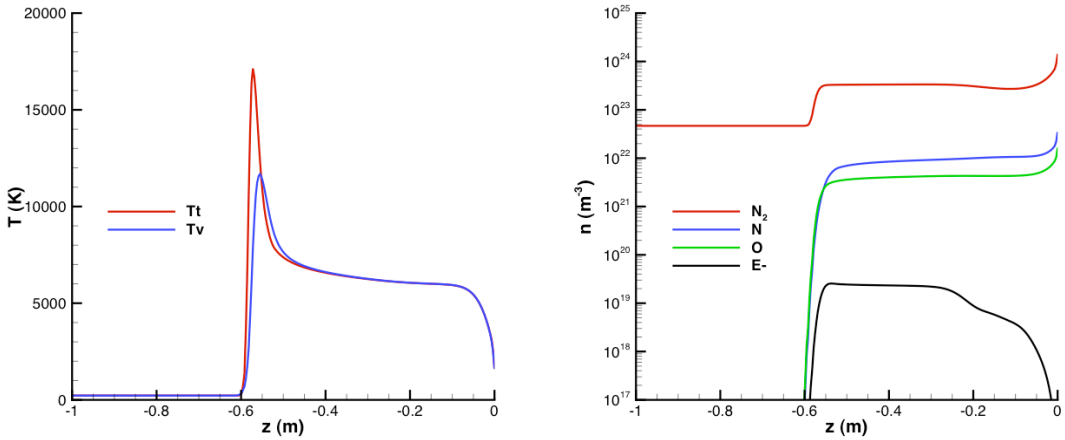

Fig. 5b: Profiles along the stagnation streamline at 75 km of: (a) temperatures; (b) selected species number densities.

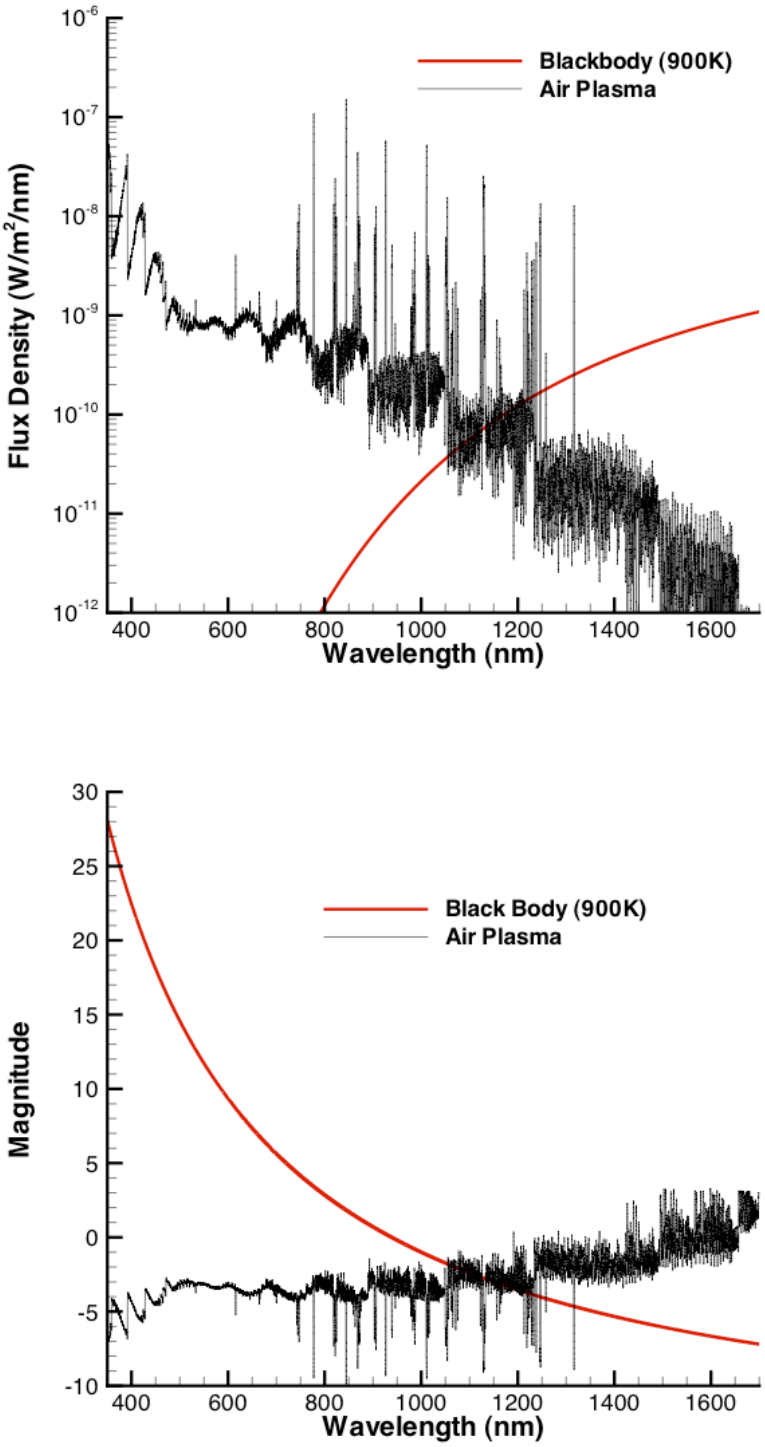

Fig. 6: Estimated radiation at 75 km: (a) flux density; (b) magnitude.

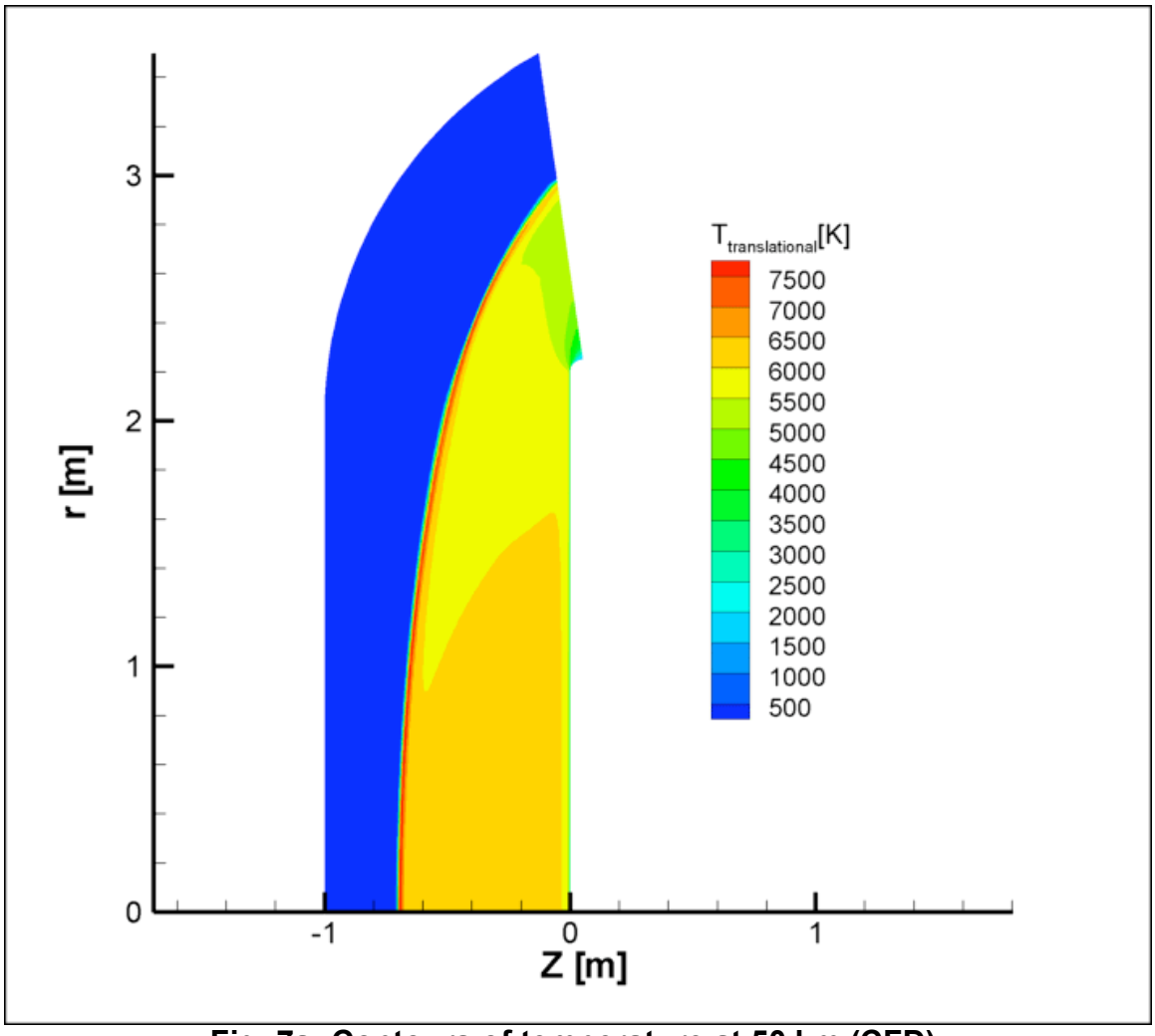

Fig. 7a: Contours of temperature at 50 km (CFD).

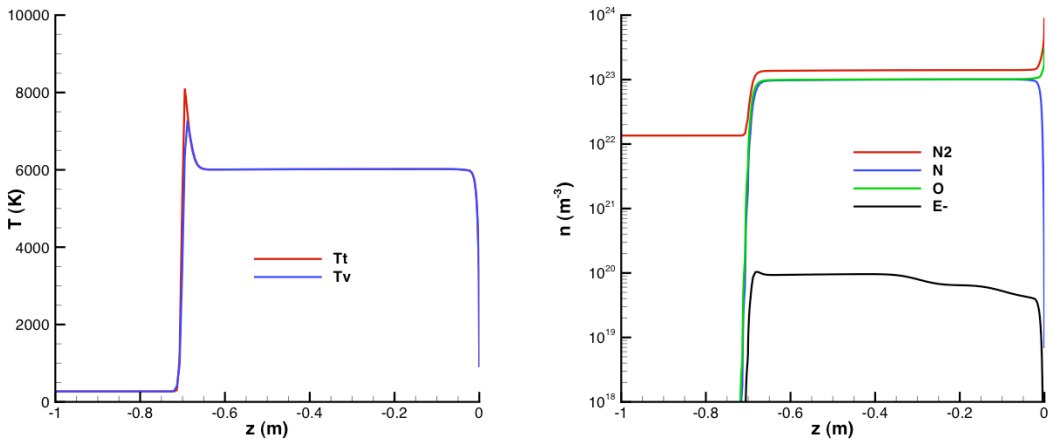

Fig. 7b: Profiles along the stagnation streamline at 50 km of: (a) temperatures; (b) selected species number densities.

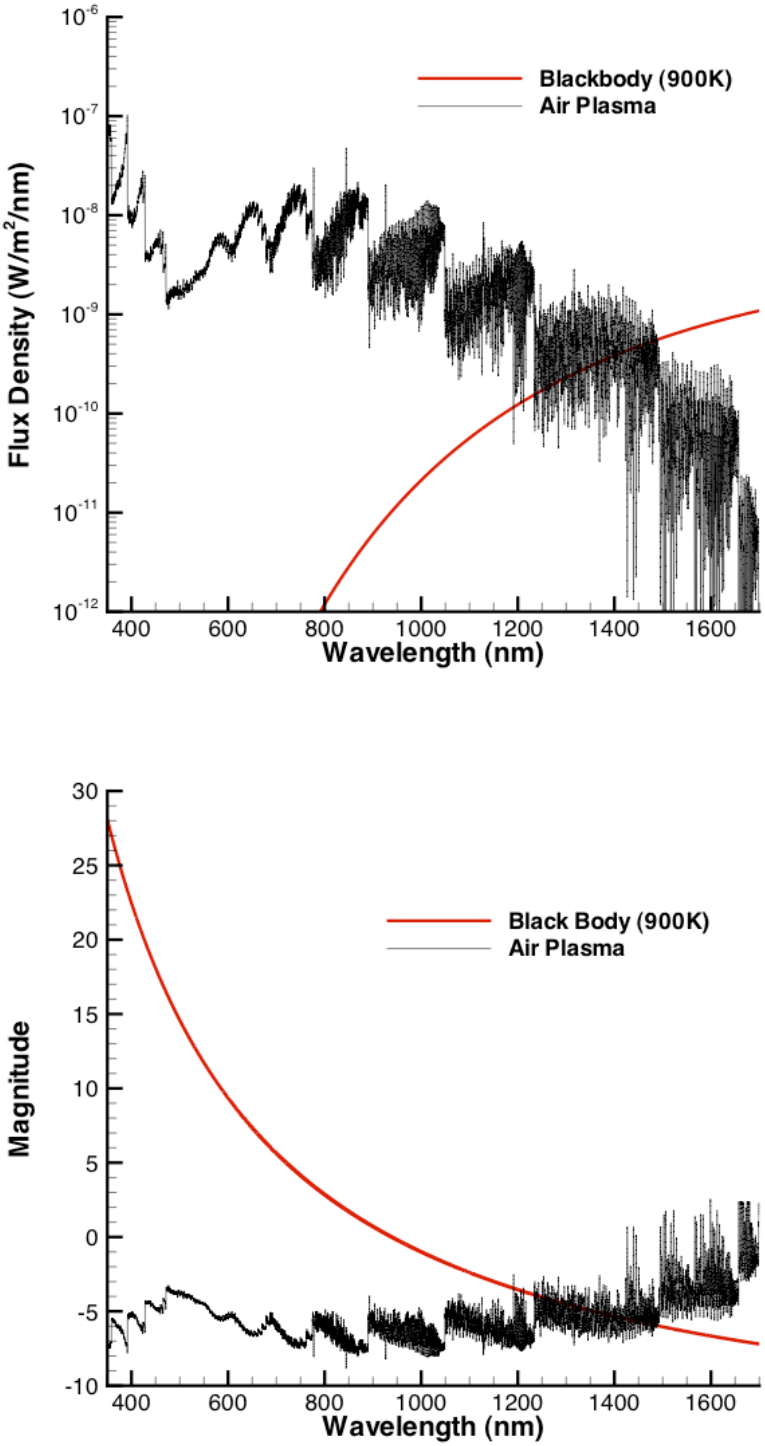

Fig. 8: Estimated radiation at 50 km: (a) flux density; (b) magnitude.